nature materials

ARTICLES

PUBLISHED ONLINE: 6 JULY 2015 | DOI: 10.1038/NMAT4340

Dislocation locking versus easy glide in titanium and zirconium

Emmanuel Clouet[1]*, Daniel Caillard[2], Nermine Chaari[1], Fabien Onimus[3] and David Rodney[4]

The ease of a metal to deform plastically in selected crystallographic planes depends on the core structure of its dislocations. As the latter is controlled by electronic interactions, metals with the same valence electron configuration usually exhibit a similar plastic behaviour. For this reason, titanium and zirconium, two transition metals of technological importance from the same column of the periodic table, have so far been assumed to deform in a similar fashion. However, we show here, using *in situ* transmission electron microscopy straining experiments, that plasticity proceeds very differently in these two metals, being intermittent in Ti and continuous in Zr. This observation is rationalized using first-principles calculations, which reveal that, in both metals, dislocations may adopt the same set of different cores that are either glissile or sessile. An inversion of stability of these cores between Zr and Ti is shown to be at the origin of the profoundly different plastic behaviours.

The favoured slip system of a crystalline metal is intimately related to the core structure of its mobile dislocations. As predicted by the famous Peierls–Nabarro model[1,2], dislocations spread or dissociated in a well-defined crystallographic plane should glide in this plane with only a very low lattice resistance. The best known example is metals with a face-centred cubic (fcc) lattice, where dislocations are dissociated in compact {111} planes in which they glide with negligible resistance[3]. The plastic behaviour of hexagonal close-packed (hcp) metals is more complex. The direction of the dominant slip system is always $\langle 1\bar{2}10\rangle$, but the associated slip plane may be either {0001} basal or $\{10\bar{1}0\}$ prismatic (see Fig. 1m for a definition of these different crystallographic planes). Selection of the dominant slip plane is known to be an electronic property[4], because the electronic structure controls the relative energies of the stacking faults in the basal and prismatic planes, which in turn determine the preferred dissociation plane for the $1/3\langle 1\bar{2}10\rangle$ dislocations.

Among hcp metals, Ti and Zr, two transition metals from group IV of the periodic table with four valence electrons, deform mainly by glide of $1/3\langle 1\bar{2}10\rangle$ dislocations in prismatic planes[5], in agreement with first-principles calculations showing that screw dislocations are stable when dissociated in their prismatic plane in both metals[6–9]. One can therefore expect that, like in fcc metals, dislocations in Ti and Zr glide in their prismatic habit plane with a negligible lattice friction. But reality is not so simple, at least in Ti. In this metal, tensile experiments[10] have shown that a lattice friction remains at low temperature ($T \leq 150$ K), even in high-purity single crystals. Transmission electron microscopy (TEM) also revealed that dislocation loops straighten along their screw orientation[11], a typical indication of a high lattice friction opposing the motion of screw dislocations. In the latter case, dislocations usually glide by the so-called Peierls mechanism[12], which involves the nucleation and propagation of kinks between neighbouring Peierls valleys. Under such conditions, the resulting dislocation motion, well known for instance in body-centred cubic (bcc) metals[5], is smooth and continuous on the timescale of *in situ* TEM straining experiments. However, during such experiments in Ti (refs 13,14), the motion of the screw dislocations is jerky and intermittent, with long time periods where the dislocations seem immobile, separated by short escape events where the dislocations glide rapidly over several Peierls valleys. Moreover, at the scale of the single crystal, the experimentally determined activation volume—that is, the variation of the strain rate with applied stress—is not consistent with a Peierls mechanism with respect to both its magnitude and stress dependence[10,13]. To rationalize these observations, a locking–unlocking mechanism has been proposed[13,14], where the screw dislocations have a sessile core in their ground state and transition to an activated metastable glissile core to move rapidly in the prismatic planes. However, the core configurations corresponding to this mechanism remain to be identified. Non-planar sessile cores have been proposed based on hypothetical dislocation dissociations[11,15,16]. More recently, *ab initio* calculations[8,9] have indicated that several configurations of the screw dislocation exist in Ti, in addition to the well-known configuration with a planar core spread in a prismatic plane, but their relative stability and ease of glide could not be evaluated. Moreover, it remains to be explained why in pure Zr, where metastable cores also exist[17,18], tensile tests on single crystals have not shown any evidence of lattice friction[19–22]. Despite the common belief that Ti and Zr have similar plastic behaviours because of their close electronic structures[5,23,24], these two metals may have in fact far less in common.

We study here the glide motion of screw dislocations in Ti and Zr, using both *in situ* TEM straining experiments and *ab initio* calculations. We show that the jerky glide in Ti is the result of a non-planar glide mechanism, where the locked periods correspond to a slow and limited glide of the dislocations in pyramidal planes and the unlocked periods to a rapid and extended glide in prismatic planes. By contrast in Zr, dislocation glide is restricted to prismatic planes, at least at the low temperatures investigated here (up to 300 K). This effect is explained by *ab initio* calculations, which show that the same dislocation cores are found in both metals, but that the most stable core in Ti, spread in a pyramidal plane, is sessile and needs to transform into a prismatic core to become glissile, whereas in Zr the prismatic glissile core is the most stable, leading to a rapid motion in this plane.

[1]CEA, DEN, Service de Recherches de Métallurgie Physique, F-91191 Gif-sur-Yvette, France. [2]CEMES-CNRS, 29 rue Jeanne Marvig, BP 94347, F-31055 Toulouse Cedex, France. [3]CEA, DEN, Service de Recherches Métallurgiques Appliquées, F-91191 Gif-sur-Yvette, France. [4]Institut Lumière Matière, Université Lyon 1, CNRS, UMR 5306, F-69622 Villeurbanne, France. *e-mail: emmanuel.clouet@cea.fr

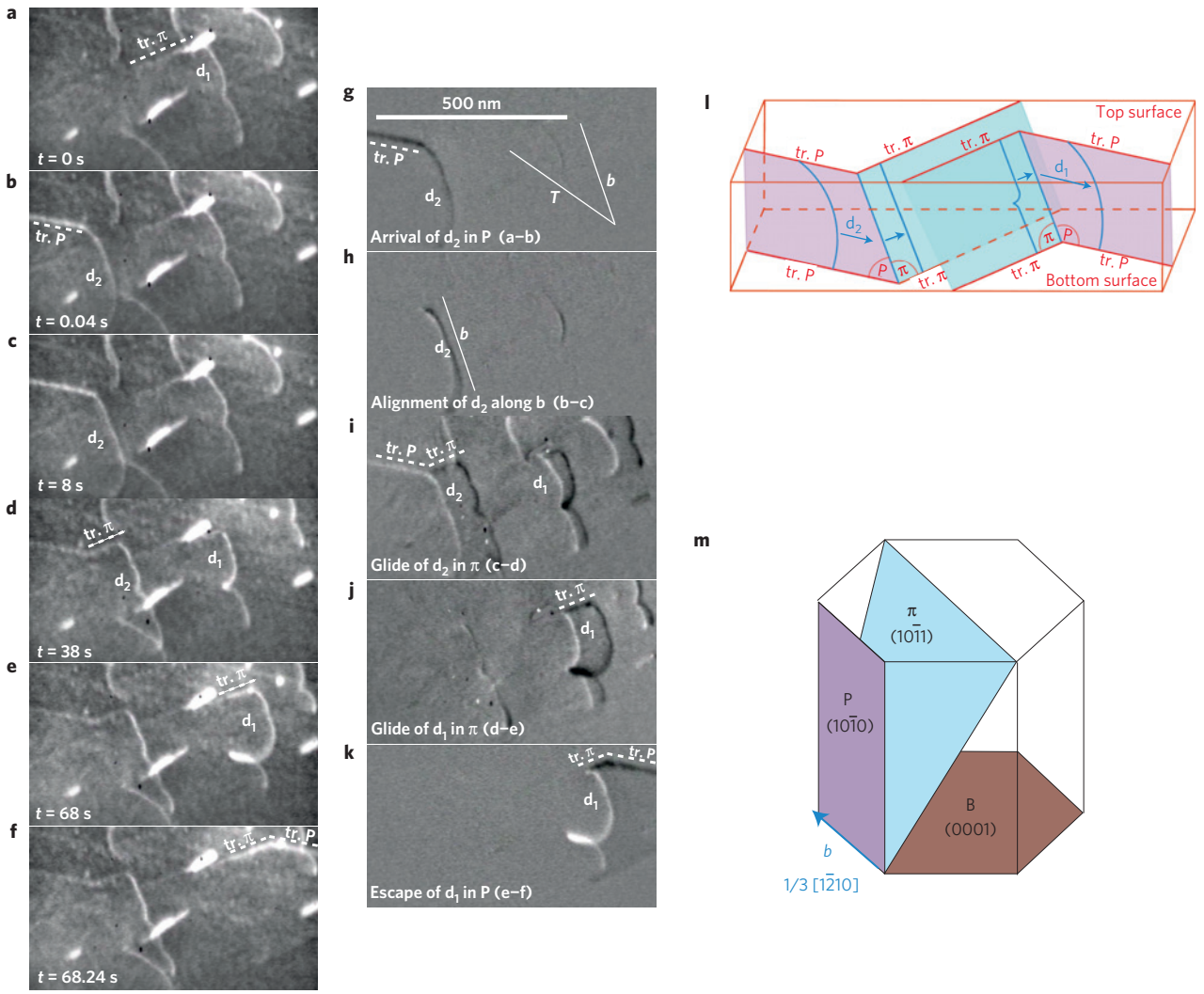

Figure 1 | Dislocation locking–unlocking mechanism in Ti at 150 K revealed by *in situ* TEM straining experiments. a–f, Successive frames following the motion of two dislocations, labelled d_1 and d_2, at different times. **g–k**, Images obtained as the difference between successive frames, showing the dislocation motion in the corresponding time interval. The dislocation d_2 arrives in the observation zone by rapid glide in a prismatic plane in less than 0.04 s (**a** and **b**), leading to the slip trace labelled 'tr. P'. It is locked between $t = 0.04$ (**b**) and 8 s (**c**). This dislocation then glides slowly in a pyramidal plane between $t = 8$ (**c**) and 38 s (**d**), leading to the slip trace 'tr. π'. The same slow glide in a pyramidal plane is observed for dislocation d_1 between $t = 8$ (**c**) and 68 s (**e**). This dislocation leaves the observation zone by rapid glide in a prismatic plane in less than 0.24 s (**e** and **f**). **l**, Sketch of dislocation glide planes and their trace on the thin foil surface. **m**, Sketch of the hexagonal unit cell.

To get a better understanding of dislocation mobility in Ti, we examine in detail the *in situ* TEM straining experiments which have been performed previously in high-purity Ti (ref. 13). Figure 1 shows a video sequence, where the ratio of Schmid factors between pyramidal and prismatic glide systems is 1.65, thus favouring pyramidal glide. The slip trace, referred as tr. π in Fig. 1a, indicates that the dislocation denoted d_1 glides in a pyramidal plane (see the inset for a three-dimensional reconstruction of the glide planes and the corresponding slip traces on the thin foil surfaces). Dislocation d_2 appearing in Fig. 1b has arrived by glide in the prismatic plane, leading to the slip trace tr. P. This prismatic glide is rapid as it happened in a time interval smaller than 40 μs, the lapse time between two successive TEM images. Dislocation d_2 then straightens up to align along its screw orientation (Fig. 1b,c), and cross-slips in a pyramidal plane (Fig. 1c,d) where it glides, but with a much smaller velocity than in the prismatic plane. Finally, dislocation d_1, which was slowly gliding in a pyramidal plane, cross-slips to rapidly escape by prismatic glide out of the observation zone, in less than 0.24 s (Fig. 1e,f).

This video sequence illustrates the locking–unlocking mechanism mentioned above. Plasticity in Ti involves a succession of locked periods where the dislocation glides slowly in pyramidal planes, separated by unlocked periods when the dislocation cross-slips in a prismatic plane and glides rapidly over large distances. The difference in velocities between prismatic and pyramidal planes indicates a large difference in lattice friction, which is also consistent with the shape of the dislocations. In pyramidal planes, the screw dislocations are straight and aligned with their Peierls valleys (see dislocation d_2 in Fig. 1c–f), a typical indication of high lattice friction, whereas in prismatic planes, the dislocations are curved, as shown in Fig. 2, which reflects a small and isotropic lattice friction despite the low temperature of these experiments (150 K). Even when the ratio of Schmid factors is closer to 1, so as to promote prismatic glide, the same jerky motion in prismatic planes with cross-slip in pyramidal planes is observed.

No such observation of dislocation motion is available for Zr. We therefore performed *in situ* TEM straining experiments in pure Zr (see Methods for details). In this metal, dislocations glide

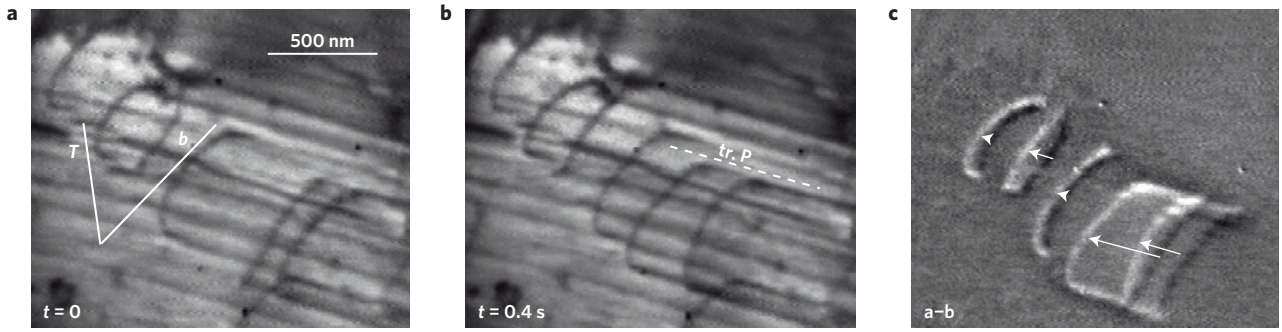

Figure 2 | Dislocation glide in a prismatic plane in Ti at 150 K. a,**b**, Same zone of the sample observed at two different times $t=0$ (**a**) and $t=0.4$ s (**b**). **c**, Frame difference between the images in **a** and **b**. The screw orientation of the dislocation is labelled *b* and the orientation *T* corresponds to the tensile axis. The slip traces caused by dislocation glide lie in a prismatic plane: they are labelled 'tr. P'.

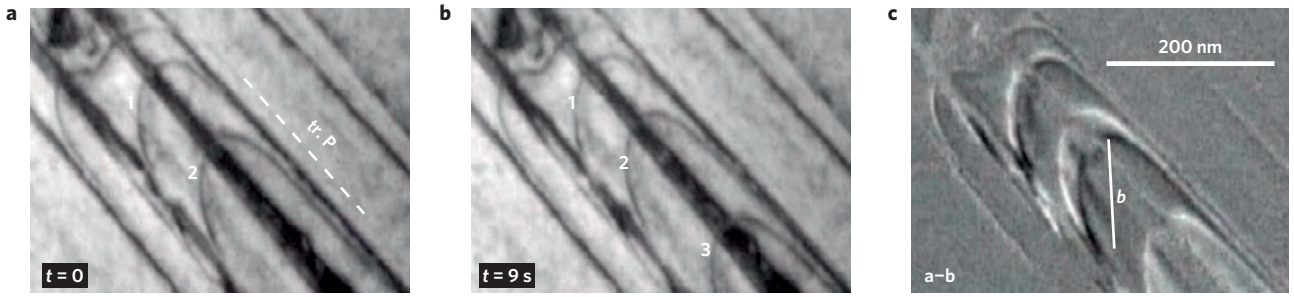

Figure 3 | Dislocation glide in a prismatic plane in Zr at 150 K. a,**b**, Same dislocations observed at two different times $t=0$ (**a**) and $t=9$ s (**b**). **c**, Frame difference between the images in **a** and **b**. The slip traces caused by dislocation glide, labelled 'tr. P', lie in a prismatic plane. The gliding dislocations are curved and do not show any straight portion in their screw orientation, denoted as *b*.

exclusively in prismatic planes between 95 and 300 K. The slip traces left on the thin foil surfaces are perfectly aligned with prismatic planes, as seen in Fig. 3 for a ratio of Schmid factors of 1.2 which should promote pyramidal glide. No cross-slip, neither in pyramidal planes nor in any other plane, is observed at these temperatures, for any sample orientations and corresponding stress levels. The dislocations gliding in the prismatic planes are curved and do not align along their screw orientation (Fig. 3). These experiments thus show that, in stark contrast to Ti, plasticity in Zr at least at low temperatures is confined in prismatic planes where the dislocations experience a negligible lattice friction.

Two different glide mechanisms are therefore observed in Ti and Zr, although both metals deform mainly by prismatic glide. To understand the origin of these different plastic behaviours, we modelled screw dislocations by *ab initio* calculations in Ti and Zr (see Methods for details). The dislocation is introduced at different positions of the atomic lattice, either as a perfect dislocation or dissociated as two partial dislocations. Atomic relaxations then lead to different configurations of the dislocation core, in agreement with previous *ab initio* calculations[8,9,17,18]. The dislocation adopts similar configurations in both metals, with the core spread either in a $\{\bar{1}011\}$ pyramidal plane (see Figs 4b,c for Ti and 5b,c for Zr) or in a $\{10\bar{1}0\}$ prismatic plane (see Figs 4d,e for Ti and 5d,e for Zr). Such spreadings are consistent with the existence of stable stacking faults in both prismatic[6–8] and pyramidal planes[17,18]. However, we find that the stabilities of these dislocation cores are opposite in both metals. Namely, our calculations show that the most stable configuration in Ti is the dislocation spread in a pyramidal plane (Fig. 4c), whereas the well-known configuration spread in a prismatic plane (Fig. 4d) is only metastable, with an excess energy of 5.7 meV Å^{-1}. In Zr, the hierarchy is reversed: the prismatic core is stable (Fig. 5d) and the pyramidal core metastable, with an excess energy of at least 2.9 meV Å^{-1} (Fig. 5a). Changing the size of the simulation box affects the excess energies, but not their ordering, neither in Ti nor in Zr.

In Ti, we therefore face the seemingly counterintuitive situation that, although the principal glide system is prismatic[5], the core spread in a prismatic plane is only metastable and less stable than the core spread in a pyramidal plane. To explain this, we consider the mobility of both cores and calculate the energy barriers between different configurations of the dislocation. We first consider in Ti the case of a dislocation in its ground state (Fig. 4c), which glides in its $\{\bar{1}011\}$ spreading pyramidal plane. We could expect, in analogy with fcc metals, a small friction as the dislocation glides in its habit plane. However, we see in Fig. 4a that the energy pathway, which corresponds to $-2 \leq \zeta \leq 0$, has a high energy barrier (11.4 meV Å^{-1}). Therefore, the glide of a dislocation in its pyramidal spreading plane is subjected to a high lattice friction, of the same order as in bcc metals[25,26], where dislocation glide is thermally activated up to room temperature and requires the nucleation and propagation of kink pairs along the dislocation lines. Another potential glide mechanism is that the dislocation first cross-slips into a prismatic plane—that is, changes its spreading plane from pyramidal to prismatic—and then glides in the prismatic plane. The energy pathway to change spreading plane, which corresponds to $0 \leq \zeta \leq 1$ in Fig. 4a, turns out to have a lower energy barrier than pyramidal glide (7.4 meV Å^{-1} compared to the 11.4 meV Å^{-1} found above). Once the dislocation is spread in a prismatic plane (Fig. 4d), it may revert to its ground state, but it may also remain in this metastable state and glide in the prismatic plane. Indeed, the barrier against glide in the prismatic plane, which corresponds to $1 \leq \zeta \leq 2$ in Fig. 4a, is very small, less than 0.4 meV Å^{-1}, meaning that the metastable core is highly mobile in the prismatic plane. If a sessile pyramidal dislocation cross-slips into a prismatic plane, it may thus remain in this metastable state and travel across several Peierls valleys in the prismatic plane until eventually thermal activation

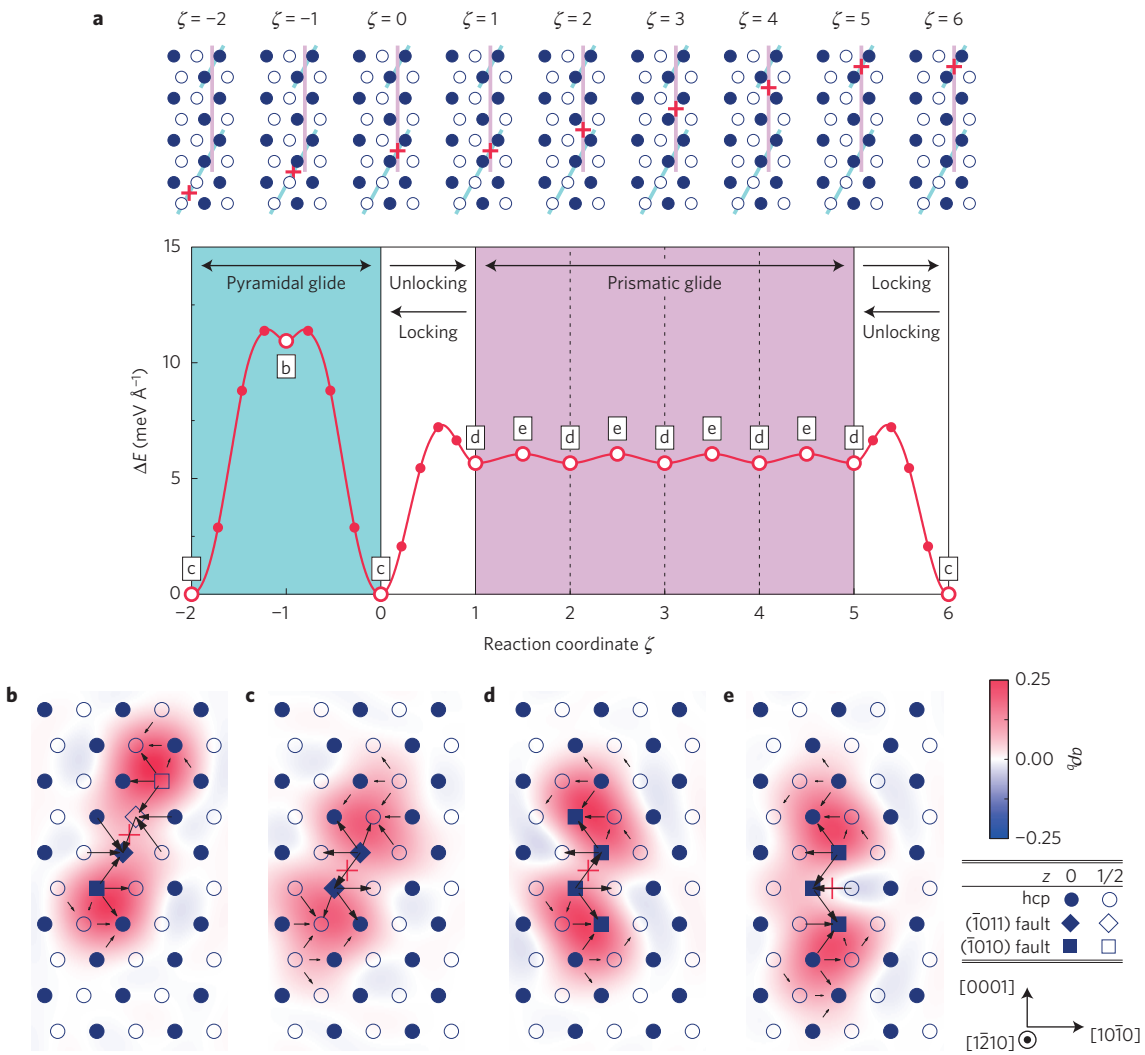

Figure 4 | *Ab initio* modelling of a screw dislocation in Ti. a, Energy barrier encountered by a screw dislocation when gliding in a $(\bar{1}011)$ pyramidal plane and when cross slipping to glide in a $(\bar{1}010)$ prismatic plane. **b–e**, Dislocation core structures for different stable and unstable equilibrium positions along the path. In these projections perpendicular to the dislocation line, atoms are sketched by symbols with a colour depending on their $(1\bar{2}10)$ plane in the original perfect crystal. Different symbols are used for atoms, depending on their neighbourhood in the dislocated crystal. The arrows between atomic columns are proportional to the differential displacement created by the dislocation in the $[1\bar{2}10]$ direction. Displacements smaller than $0.1b$ are not shown. The contour map shows the dislocation density ρ_b normalized by the inverse of the lattice parameter a. The red cross indicates the dislocation position.

brings it back to its pyramidal ground state. The above *ab initio* calculations thus fully confirm the locking–unlocking mechanism proposed to explain the *in situ* TEM observation of jerky glide in Ti. In their ground state, screw dislocations are spread in a pyramidal plane and have a low mobility as seen *in situ* because of the high lattice friction in these planes. However, if they transform into a metastable glissile core spread in a prismatic plane, they can glide over long distances with a very low migration barrier, resulting in a prismatic glide plane for the main slip system.

In Zr, the situation is simpler because the most stable configuration is spread in a prismatic plane (Fig. 5d) and the energy barrier to glide in this plane, which corresponds to $0 \leq \zeta \leq 2$ in Fig. 5a, is negligible, in agreement with previous *ab initio* calculations[7] that showed that the corresponding Peierls stress does not exceed 21 MPa. No locking–unlocking mechanism is therefore needed in Zr to activate prismatic slip, and dislocation glide is smooth and continuous, as observed in our *in situ* TEM experiments. Screw dislocations can still cross-slip to a metastable state partially spread in a pyramidal plane[17,18], as described by $-1 \leq \zeta \leq 0$ in Fig. 5a, but glide in this plane is subjected to a high energy barrier. The pathway, which corresponds to $-5 \leq \zeta \leq -3$ in Fig. 5a, goes through another metastable state of higher energy, also spread in the pyramidal plane (Fig. 5c) with an energy barrier of 8 meV Å^{-1}. If a prismatic dislocation cross-slips in a pyramidal plane, it will most likely fall back into its ground state (pathway with $-2 \leq \zeta \leq -1$) as the energy barrier is much smaller (3.5 meV Å^{-1}). We thus anticipate that pyramidal glide in Zr is activated only at high temperatures, with dislocation glide confined to prismatic planes at low temperatures, which explains why only prismatic glide was observed in our straining experiments performed below 300 K.

The distinct plastic behaviour of Ti and Zr is therefore related to a different stability of the various dislocation configurations. This stability is not simply controlled by the values of the stacking fault energies. In both metals, the stacking fault in the pyramidal plane costs less energy than the stacking fault in the prismatic plane[17]: the stacking fault energies in the pyramidal and prismatic planes are respectively 227 and 256 mJ m^{-2} in Ti, and 163 and 211 mJ m^{-2} in Zr. These stacking faults are responsible for the dislocation dissociation seen in the atomistic simulations (Figs 4b–e and 5b–e): for the pyramidal configuration, the two partial dislocations have

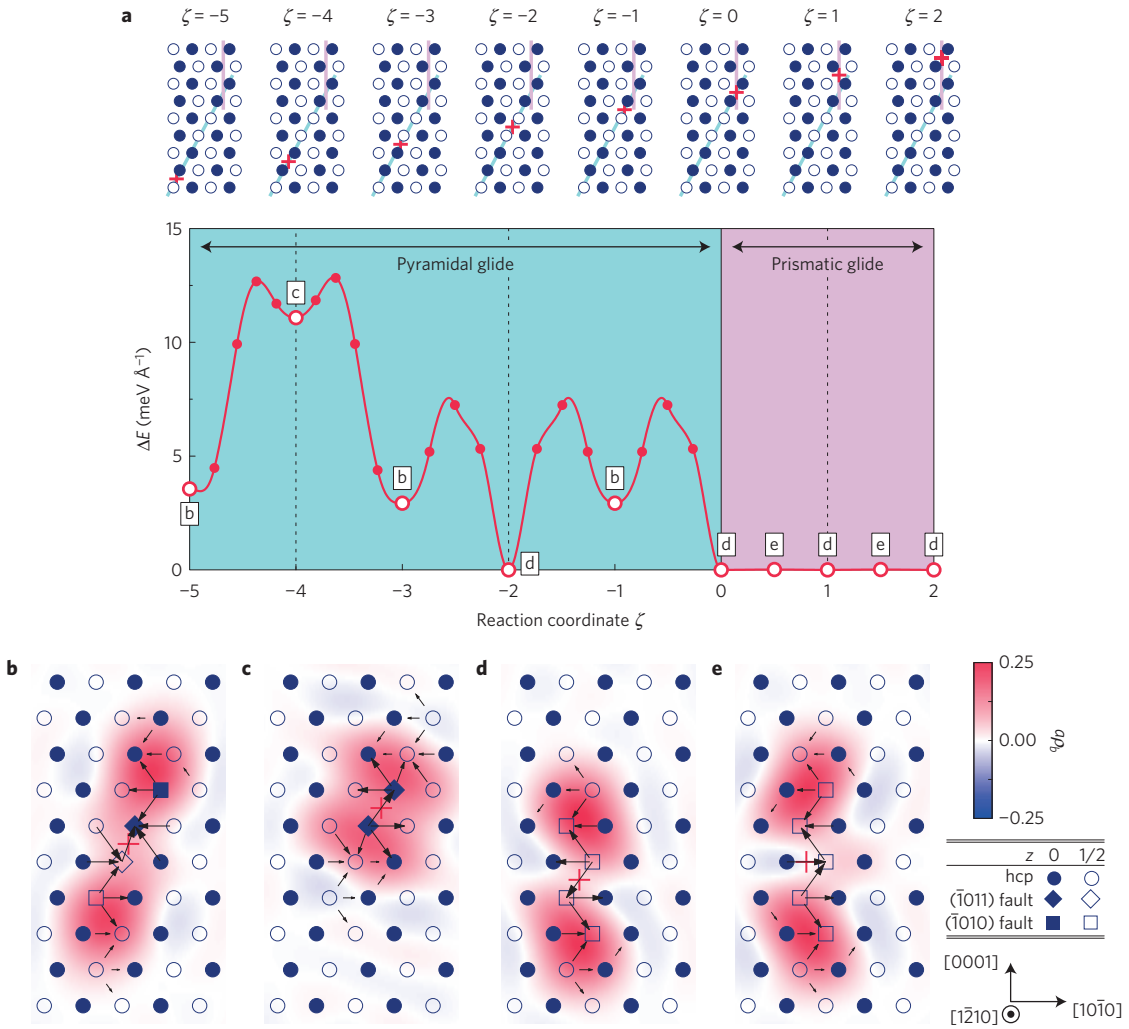

Figure 5 | *Ab initio* modelling of a screw dislocation in Zr. a, Energy barrier encountered by a screw dislocation when gliding either in a $(\bar{1}011)$ pyramidal plane or in a $(\bar{1}010)$ prismatic plane. **b**–**e**, Corresponding dislocation core structures (see Fig. 4 for a detailed description).

Burgers vectors $1/6\,[1\bar{2}10] \pm (4\gamma^2-9)/2(4\gamma^2+3)\,[10\bar{1}2]$, and for the prismatic configuration they have the same $1/6\,[1\bar{2}10]$ Burgers vectors (γ is the c/a ratio). According to anisotropic elasticity theory, the corresponding dissociation distances for the pyramidal and prismatic configurations are respectively 5.3 and 5.5 Å in Ti, and 5.9 and 6.1 Å in Zr (see Methods for calculation details). The dislocation splitting, corresponding roughly to $1.8a$ in both metals, is slightly higher than the interatomic distance, in agreement with the dislocation densities extracted from the atomistic simulations (Figs 4b–e and 5b–e), but the different splitting distances obtained between the pyramidal and prismatic configurations do not lead to a significant variation of dissociation energy which could explain the reverse stabilities predicted by the *ab initio* calculations.

To understand the different stability of dislocations in Ti and Zr, we analyse the local density of states (LDOS) in the pyramidal and prismatic configurations—that is, the respective ground states in Ti and Zr (see Methods for details). As already pointed by Tarrat *et al.*[9], the screw dislocation induces an increase of the number of high-energy occupied states close to the Fermi level. Variations of the LDOS are observed between both dislocation configurations, but this variation between Ti and Zr is significant only for the two atoms located in the immediate vicinity of the dislocation centre. These two atoms have a changing neighbouring between the two core structures, corresponding either to a pyramidal (Fig. 4c) or a prismatic stacking fault (Fig. 4d). In Ti, the pseudo-gap at the Fermi level of the LDOS on these atoms is more pronounced for the pyramidal than for the prismatic configuration (Fig. 6a), thus leading to a stabilization of the pyramidal configuration by the corresponding band energy. The inverse is observed in Zr (Fig. 6b), in agreement with the total energy calculations. As the stability of the dislocation pyramidal configuration is related to subtle variations in the LDOS, it is not surprising that empirical interatomic potentials, such as the embedded atom method (EAM) or modified EAM, fail to predict the correct dislocation ground state in Ti (refs 8,9,27). These LDOS also show that electron doping by addition of alloying elements should slightly decrease the energy difference between the dislocation configurations in both cases, thus favouring prismatic glide in Ti and enhancing pyramidal cross-slip in Zr.

Both *ab initio* and *in situ* TEM straining experiments show that in Ti, prismatic glide proceeds via a locking–unlocking mechanism, whereas in Zr, no significant lattice friction is involved. The same configurations of the screw dislocation exist in both metals, but different relative stabilities result in strikingly distinct plastic behaviours. Titanium, in particular, constitutes an unusual case where the glide plane of the main slip system differs from the habit plane of the dislocations in their ground state. Plasticity in these hcp metals can only be understood if we consider the relative stability of the different potential dislocation configurations, in stark contrast to fcc or bcc metals, where the plastic behaviour mainly results from a single dislocation configuration. With such an understanding

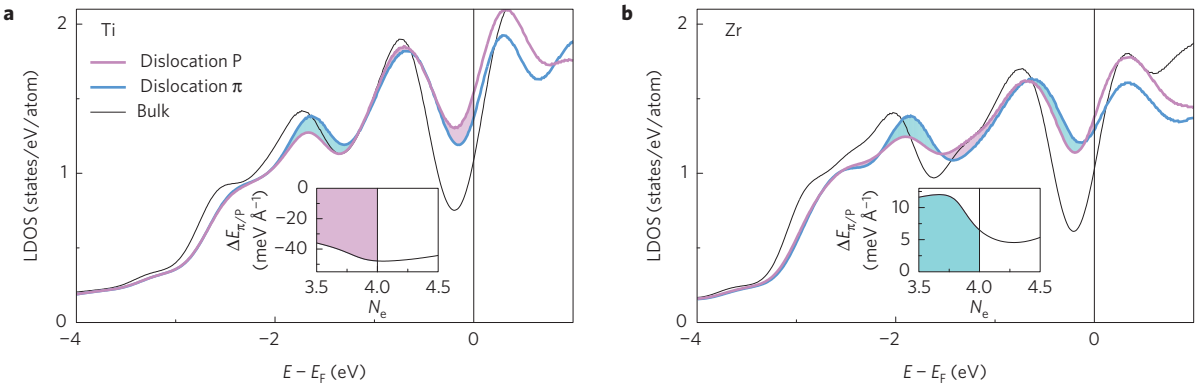

Figure 6 | Electronic density of states in Ti and Zr. a,**b**, Local density of states on the two atoms located in the immediate vicinity of the dislocation centre for the prismatic and pyramidal dislocation configurations, and compared to the density of states in the perfect crystal. The insets show the corresponding energy difference between the pyramidal and prismatic configurations, $\Delta E_{\pi/P}$, for a varying number N_e of valence electrons.

of dislocation glide properties in the pure Ti and Zr metals, it will now be possible to address plasticity in alloys, by looking at how alloying elements affect the stability of the various dislocation cores encountered here. In particular, interstitial elements such as oxygen are known to induce a strong hardening in both Ti and Zr. Previous studies have shown that this hardening cannot be associated with simple elastic interactions between dislocations and solutes[11,28]. A possibility for such hardening may then be a locking of the dislocations in their sessile configuration induced by the solute atoms. Substitutional alloying elements, by changing the Fermi level, should also impact the plastic behaviour.

Methods

Methods and any associated references are available in the online version of the paper.

Received 22 January 2015; accepted 29 May 2015; published online 6 July 2015

References

1. Peierls, R. The size of a dislocation. *Proc. Phys. Soc.* **52,** 34–37 (1940).
2. Nabarro, F. R. N. Dislocations in a simple cubic lattice. *Proc. Phys. Soc.* **59,** 256–272 (1947).
3. Hirth, J. P. & Lothe, J. *Theory of Dislocations* 2nd edn (Wiley, 1982).
4. Legrand, B. Relation between the electronic structure and ease of gliding in hexagonal close-packed metals. *Philos. Mag. B* **49,** 171–184 (1984).
5. Caillard, D. & Martin, J. L. *Thermally Activated Mechanisms in Crystal Plasticity* (Pergamon, 2003).
6. Domain, C. *Ab initio* modelling of defect properties with substitutional and interstitials elements in steels and Zr alloys. *J. Nucl. Mater.* **351,** 1–19 (2006).
7. Clouet, E. Screw dislocation in zirconium: An *ab initio* study. *Phys. Rev. B* **86,** 144104 (2012).
8. Ghazisaeidi, M. & Trinkle, D. Core structure of a screw dislocation in Ti from density functional theory and classical potentials. *Acta Mater.* **60,** 1287–1292 (2012).
9. Tarrat, N. *et al.* Screw dislocation in hcp Ti: DFT dislocation excess energies and metastable core structures. *Modelling Simul. Mater. Sci. Eng.* **22,** 055016 (2014).
10. Biget, M. P. & Saada, G. Low-temperature plasticity of high-purity α-titanium single crystals. *Philos. Mag. A* **59,** 747–757 (1989).
11. Naka, S., Lasalmonie, A., Costa, P. & Kubin, L. P. The low-temperature plastic deformation of α titanium and the core structure of a-type screw dislocations. *Philos. Mag. A* **57,** 717–740 (1988).
12. Guyot, P. & Dorn, J. E. A critical review of the Peierls mechanism. *Can. J. Phys.* **45,** 983–1016 (1967).
13. Farenc, S., Caillard, D. & Couret, A. An *in situ* study of prismatic glide in α titanium at low temperatures. *Acta Metall. Mater.* **41,** 2701–2709 (1993).
14. Farenc, S., Caillard, D. & Couret, A. A new model for the peak of activation area of α titanium. *Acta Metall. Mater.* **43,** 3669–3678 (1995).
15. Šob, M., Kratochvíl, J. & Kroupa, F. Theory of strengthening of alpha titanium by interstitial solutes. *Czech. J. Phys. B* **25,** 872–890 (1975).
16. Naka, S., Kubin, L. P. & Perrier, C. The plasticity of titanium at low and medium temperatures. *Philos. Mag. A* **63,** 1035–1043 (1991).
17. Chaari, N., Clouet, E. & Rodney, D. First-principles study of secondary slip in zirconium. *Phys. Rev. Lett.* **112,** 075504 (2014).
18. Chaari, N., Clouet, E. & Rodney, D. First order pyramidal slip of $1/3\langle 1\bar{2}10\rangle$ screw dislocations in zirconium. *Metall. Mater. Trans. A* **45,** 5898–5905 (2014).
19. Rapperport, K. E. J. & Hartley, C. S. Deformation modes of zirconium at 77°, 575°, and 1075°K. *Trans. Am. Inst. Min. Eng.* **218,** 869–876 (1960).
20. Mills, D. & Craig, G. B. The plastic deformation of zirconium–oxygen alloy single crystals in the range 77 to 950 K. *Trans. Am. Inst. Min. Eng.* **242,** 1881–1890 (1968).
21. Soo, P. & Higgins, G. T. The deformation of zirconium–oxygen single crystals. *Acta Metall.* **16,** 177–186 (1968).
22. Akhtar, A. & Teghtsoonian, A. Plastic deformation of zirconium single crystals. *Acta Metall.* **19,** 655–663 (1971).
23. Bacon, D. & Vitek, V. Atomic-scale modeling of dislocations and related properties in the hexagonal-close-packed metals. *Metall. Mater. Trans. A* **33,** 721–733 (2002).
24. Kubin, L. *Dislocations, Mesoscale Simulations and Plastic Flow* (Oxford Series on Materials Modelling, Oxford University Press, 2013).
25. Weinberger, C. R., Tucker, G. J. & Foiles, S. M. Peierls potential of screw dislocations in bcc transition metals: Predictions from density functional theory. *Phys. Rev. B* **87,** 054114 (2013).
26. Dezerald, L. *et al. Ab initio* modeling of the two-dimensional energy landscape of screw dislocations in bcc transition metals. *Phys. Rev. B* **89,** 024104 (2014).
27. Rao, S., Venkateswaran, A. & Letherwood, M. Molecular statics and molecular dynamics simulations of the critical stress for motion of $a/3\langle 11\bar{2}0\rangle$ screw dislocations in α-Ti at low temperatures using a modified embedded atom method potential. *Acta Mater.* **61,** 1904–1912 (2013).
28. Yu, Q. *et al.* Origin of dramatic oxygen solute strengthening effect in titanium. *Science* **347,** 635–639 (2015).

Acknowledgements

This work was performed using HPC resources from GENCI-CINES, -TGCC and -IDRIS (Grant 2014-096847). The authors also acknowledge PRACE for awarding them access to the Curie resources based in France at TGCC (project PlasTitZir). They are grateful to D. Chaubet and J.-L. Béchade for processing the initial zirconium Van Arkel material. They also want to thank B. Arnal for his help in specimen preparation, and B. Legrand and F. Willaime for fruitful discussions.

Author contributions

E.C. and N.C. performed the *ab initio* calculations with the help of D.R.; D.C. performed the *in situ* TEM straining experiments; and F.O. prepared the Zr samples for these experiments. E.C., D.C. and D.R. prepared the manuscript. All the authors discussed the results and reviewed the paper.

Additional information

Reprints and permissions information is available online at www.nature.com/reprints. Correspondence and requests for materials should be addressed to E.C.

Competing financial interests

The authors declare no competing financial interests.

Methods

***Ab initio* calculations.** *Ab initio* calculations are performed with the Pwscf code[29], using the exchange–correlation functional of Perdew, Burke and Ernzerhof[30] and the pseudopotential approximation. The pseudopotential is ultrasoft of Vanderbilt type with 3*s* and 3*p* electrons included as semi-core for Ti, and 4*s* and 4*p* electrons for Zr. Electronic wavefunctions are expanded in plane waves using a cutoff energy of 48 Ry for Ti and 28 Ry for Zr, and a regular grid of $2\times2\times14$ k-points in Ti and $2\times1\times14$ k-points in Zr. The electronic density of states is broadened with the Methfessel–Paxton function using a spreading of 22 mRy.

Dislocations are modelled in simulation cells with fully periodic boundary conditions. Two dislocations of opposite Burgers vectors are introduced in the simulation cell. Their positions are chosen so as to form a quadrupolar periodic array of dislocations, which minimizes the elastic interaction between the dislocations and their images. Because of the centrosymmetry of the Volterra elastic field, such a quadrupolar arrangement ensures that the stress field created by the periodic image dislocations cancels locally at each dislocation position, thus limiting the perturbation of the dislocation core by the boundary conditions. The chosen array was described as an S arrangement in ref. 7. The periodicity vectors of the simulation cell, before introduction of the dislocation dipole, are $\mathbf{a}_x = n\,a[10\bar{1}0]$, $\mathbf{a}_y = m\,c[0001]$ and $\mathbf{a}_z = \mathbf{b} = 1/3\,a[1\bar{2}10]$, where n and m are two integers. Results presented in Figs 4 and 5 were obtained with $n=6$ and $m=8$, corresponding to 192 atoms. Similar results are obtained with 6×6 and 8×8 simulation cells in Ti, and with 4×6, 4×8, 5×6 and 5×8 simulation cells in Zr. Dislocation stable and unstable equilibrium configurations (Figs 4b–e and 5b–e) are obtained after relaxation of the atomic positions with a tolerance of 2 meV Å^{-1} for atomic forces.

Energy barriers corresponding to dislocation cross-slip or glide are obtained with the nudged elastic band method[31] using three or four intermediate images. The tolerance on atomic forces is 20 meV Å^{-1}. Excess energies, with periodic boundary conditions, are simply given by the energy difference between configurations calculated in the same simulation box, thus assuming a constant elastic energy along the pathways. This assumption is valid when the separation distance between the two dislocations composing the dipole does not vary, which was checked in our simulations.

Local densities of states (LDOS) $n(E)$ are obtained by projecting the electronic wavefunctions onto orthogonalized atomic wavefunctions. The band energy E^{b} is then defined[32] by $E^{\mathrm{b}} = \int^{E_{\mathrm{F}}} n(E)(E-E_{\mathrm{F}})\mathrm{d}E$, with the Fermi energy E_{F} linked to the number of valence electrons N_{e} by $N_{\mathrm{e}} = \int^{E_{\mathrm{F}}} n(E)\mathrm{d}E$. In Fig. 6, only the two atoms in the immediate vicinity of the dislocation core are considered in the band energy calculation: these atoms correspond to the two filled diamonds in Fig. 4c and to the two filled squares close to the dislocation centre in Fig. 4d. The difference in dislocation energies is given by $\Delta E_{\pi/\mathrm{P}} = 2(E^{\mathrm{b}}_{\pi} - E^{\mathrm{b}}_{\mathrm{P}})/b$, with E^{b}_{π} and $E^{\mathrm{b}}_{\mathrm{P}}$ computed for the LDOS corresponding to the pyramidal and prismatic dislocation configurations, respectively.

Visualization of dislocation core structure. Contour maps of the dislocation density are deduced from the screw component along the $[1\bar{2}10]$ direction of the Nye tensor. This tensor is extracted from our simulations using the method of Hartley and Mishin[33]. For this post-processing treatment, the neighbourhood of each atom is defined by a sphere of radius 1.3 times the lattice parameter. This neighbourhood is identified with one of the following perfect patterns: same neighbourhood in a perfect hcp lattice, in an unrelaxed prismatic stacking fault, and in a perfect hcp lattice after a $(\bar{1}011)$ mirror symmetry corresponding to the neighbourhood inside the unrelaxed pyramidal stacking fault[17,18]. The angle threshold on atomic bonds used for this identification step is 10°.

Dislocation dissociation. Anisotropic elasticity theory predicts that screw dislocations dissociate in prismatic and pyramidal planes with a splitting distance d minimizing the dissociation energy

$$\Delta E_{\mathrm{diss}}(d) = \left[{b_e}^2 \left(\frac{3}{3+4\gamma^2} K_{11} + \frac{4\gamma^2}{3+4\gamma^2} K_{22} \right) - \frac{1}{4} a^2 K_{33} \right] \log\left(\frac{d}{r_{\mathrm{c}}}\right) + \sigma d$$

where γ is the c/a ratio, σ the stacking fault energy, r_{c} a dislocation core radius, and b_e the edge component of the Burgers vector lying in the $(10\bar{1}1)$ plane: $b_e = 0$ for the prismatic configuration and $b_e = a(4\gamma^2-9)/2\sqrt{3+4\gamma^2}$ for the pyramidal configuration[17]. An expression for the Stroh matrix $\overline{\overline{K}}$ as a function of the elastic constants C_{ij} can be found in ref. 7, with the parameters used for Zr. For Ti, our *ab initio* calculations lead to $a = 2.936$ Å, $\gamma = 1.583$, $C_{11} = 169$, $C_{12} = 89$, $C_{33} = 192$, $C_{13} = 77$ and $C_{44} = 42$ GPa.

Experiments. *In situ* TEM straining experiments in titanium were performed by Farenc *et al.*[13] using a home-made low-temperature holder and 200CX transmission electron microscope. The high-purity titanium studied in these experiments is that used by Biget and Saada[10] in their tensile tests on single crystals. It contains only 50 atomic parts per million (appm) O and 70–100 appm Fe.

The new *in situ* experiments carried out in zirconium between 95 and 300 K were performed with a Gatan low-temperature straining holder and a JEOL 2010HC transmission electron microscope. The zirconium samples contain 1.1 at.% Hf, 600 appm O, 600 appm C, 50 appm N and 800 appm Fe.

References

29. Giannozzi, P. *et al.* QUANTUM ESPRESSO: A modular and open-source software project for quantum simulations of materials. *J. Phys. Condens. Matter* **21,** 395502 (2009).
30. Perdew, J. P., Burke, K. & Ernzerhof, M. Generalized gradient approximation made simple. *Phys. Rev. Lett.* **77,** 3865–3868 (1996).
31. Henkelman, G. & Jónsson, H. Improved tangent estimate in the nudged elastic band method for finding minimum energy paths and saddle points. *J. Chem. Phys.* **113,** 9978–9985 (2000).
32. Ducastelle, F. *Order and Phase Stability in Alloys* (North-Holland, 1991).
33. Hartley, C. S. & Mishin, Y. Characterization and visualization of the lattice misfit associated with dislocation cores. *Acta Mater.* **53,** 1313–1321 (2005).